Use of gene expression profiling to direct *in vivo* molecular imaging of lung cancer

Jan Grimm*†, David G. Kirsch†‡§, Stephen D. Windsor*, Carla F. Bender Kim§, Philip M. Santiago§, Vasilis Ntziachristos*, Tyler Jacks§¶, and Ralph Weissleder*‖

*Center for Molecular Imaging Research and ‡Department of Radiation Oncology, Massachusetts General Hospital and Harvard Medical School, Charlestown, MA 02129; and §Department of Biology and Center for Cancer Research and ¶Howard Hughes Medical Institute, Massachusetts Institute of Technology, Cambridge, MA 02139

Edited by George Klein, Karolinska Institutet, Stockholm, Sweden, and approved August 23, 2005 (received for review May 11, 2005)

Using gene expression profiling, we identified cathepsin cysteine proteases as highly up-regulated genes in a mouse model of human lung adenocarcinoma. Overexpression of cathepsin proteases in these lung tumors was confirmed by immunohistochemistry and Western blotting. Therefore, an optical probe activated by cathepsin proteases was selected to detect murine lung tumors *in vivo* as small as 1 mm in diameter and spatially separated. We generated 3D maps of the fluorescence signal and fused them with anatomical computed tomography images to show a close correlation between fluorescence signal and tumor burden. By serially imaging the same mouse, optical imaging was used to follow tumor progression. This study demonstrates the capability for molecular imaging of a primary lung tumor by using endogenous proteases expressed by a tumor. It also highlights the feasibility of using gene expression profiling to identify molecular targets for imaging lung cancer.

Mouse models of human cancer have dramatically improved over the past decade. It is now possible to introduce mutations identical to those commonly found in human cancer into the endogenous murine gene locus, improving the physiological relevance. Moreover, the incorporation of conditional mutation systems, such as the Cre-lox system (1), allows tumor initiation in these mouse models to be regulated temporally and spatially. Therefore, an oncogene or tumor suppressor gene can be examined in a specific tissue and developmental stage that is most relevant to the human cancer under study.

We have previously described a mouse model of human lung adenocarcinoma that is initiated by Cre recombinase (2). LSL-KrasG12D mice carry a conditional mutation (G12D) in the K-ras oncogene; this codon is frequently mutated in human lung adenocarcinoma (3–5). The mutant allele is not expressed because of the presence of a transcriptional STOP cassette upstream of exon 1 (6). In the presence of Cre recombinase, the STOP cassette is deleted, and oncogenic K-rasG12D is expressed from the endogenous K-ras promoter at physiological levels. Intranasal instillation of adenovirus that expresses Cre recombinase results in infection of respiratory epithelia and subsequent expression of oncogenic K-ras. These mice develop lung adenomas that progress into lung adeoncarcinomas (2). The K-ras^{G12D} lung tumors not only resemble human tumors at the molecular level but also appear similar histologically. Moreover, we have characterized the gene expression profile of K-ras^{G12D} lung tumors generated by a similar strategy (7) and found that the profile is similar to that of human lung adenocarcinomas (8). Interestingly, a pattern of gene expression indicative of mutant K-ras was identified by cross-species gene expression studies between murine and human lung adenocarcinomas (8). This oncogenic K-ras gene expression signature was not apparent when the human lung tumors were analyzed alone. Therefore, this mouse model has been useful in informing us about the molecular nature of human lung cancer.

While new approaches to mouse modeling have taken place over the past decade, parallel advances have occurred in molecular imaging, which characterizes and measures molecular events in living animals with high sensitivity and spatial resolution (9). Imaging these molecular events is achieved by using innovative imaging agents, including "smart sensor probes" that can be activated upon interaction with their biological targets (10). The progress of molecular imaging has been accelerated by the development of dedicated small animal imaging equipment for micro-computed tomography (CT) and optical imaging. Optical imaging has seen exciting achievements in recent years, such as the development of optical tomography, which, in contrast to reflectance imaging, is not surface-weighted (11, 12). One technique, fluorescence molecular tomography (FMT), is capable of resolving molecular functions in deep tissues by reconstructing the *in vivo* distribution of i.v. injected far red and near infrared fluorescent probe (13).

Here, we combine information from the gene expression profile studies of murine lung cancers with advances in optical imaging and micro-CT. Gene expression profiles of K-ras^{G12D} tumors identified several cathepsin proteases as genes that are strongly up-regulated in lung tumors compared with normal lung tissue. These proteases are also overexpressed in some patients with lung cancer, and their expression has been associated with tumor invasion and poor prognosis (14, 15). We hypothesized that tumor protease activity could be used as a means of detecting these tumors. Furthermore, we reasoned that the noninvasive imaging method could provide a powerful tool to study protease activity during tumor initiation and progression. Our data confirm that protease activity in primary lung tumors can indeed be resolved with optical tomography. Furthermore, we demonstrate that FMT is sensitive in detecting small tumors and can be used to follow tumor progression. This study exemplifies how gene expression profiles can be used to select innovative imaging approaches for cancer with the combination of functional and anatomical imaging.

Materials and Methods

Animal Model. Wild-type, *LSL-KrasG12D*, or LSL-KrasG12D;LSL-p53R270H/Flox (16) mice were infected with an adenovirus expressing Cre recombinase (Adeno-Cre) by intranasal instillation as described in ref. 2. Adeno-Cre was purchased from the University of Iowa Gene Transfer Vector Core (Iowa City).

FMT. FMT was acquired by using a continuous wave-type scanner capable of acquiring transillumination, reflectance, and absorption data (FMT, VisEn Medical, Woburn, MA). Prototypes of

This paper was submitted directly (Track II) to the PNAS office.

Abbreviations: CT, computed tomography; FMT, fluorescence molecular tomography; Adeno-Cre, adenovirus expressing Cre recombinase; IHC, immunohistochemistry.

†J.G. and D.G.K. contributed equally to this work.

‖To whom correspondence should be addressed. E-mail: weissleder@helix.mgh.harvard.edu.

www.pnas.org/cgi/doi/10.1073/pnas.0503920102

Table 1. Ratios of cathepsin H, B, and L gene expression in 31 lung tumors compared with 19 normal lungs from mice that do not have lung tumors as previously reported in ref. 8

Gene	Tumor/normal ratio
Cathepsin H	3.8
Cathepsin B	2.6
Cathepsin L	1.2

the device and reconstruction algorithms are described in more detail in ref. 17.

All mice were anesthetized with isoflurane inhalation narcosis during FMT imaging. Twenty-four hours before imaging, the mice were injected i.v. with 2 nmol of an intravital cysteine protease probe (Prosense 680, VisEn Medical), a cathepsin activatable probe with an excitation wavelength of 680 nm and an emission wavelength of 720 nm. Before imaging, the mice were shaved to reduce the influence of the fur on the optical signal.

3D volume-rendered reconstructions of the acquired data set were produced by using OSIRIX (18) to demonstrate the 3D distribution of the signal from the activated probe and to compare it with the anatomical location of the bulk tumor mass in CT. Coronal FMT images were manually coregistered with corresponding coronal CT slices by using the sagittal position of the slice on CT as well as FMT for orientation. The images were fused to obtain CT-FMT fusion images, showing both molecular function (cathepsin activity) and anatomical structure (tumors) in one image.

After the mice were killed, lungs and other organs were excised and imaged in surface-reflectance mode to confirm the origin of the signal from the tumors. Individual tumors were isolated from the lung and again imaged to measure signal intensity. These tumors were homogenized and snap-frozen for later analysis of cathepsin expression. Correlation of tumor size obtained with CT was compared with the size obtained from histology by using PRISM (GraphPad, San Diego).

CT. CT data were acquired on a combined high-resolution single-photon emission CT (SPECT)-CT scanner (Gamma-Medica X-SPECT, Northridge, CA) equipped with a dual-gamma camera SPECT system and x-ray fan beam CT scanner. The x-ray tube produces medium-energy x-rays of 50 keV with 500-mA current. Each CT scan acquires 256 single projections; reconstructions are performed by using filtered back-projections. Secondary multiplanar and 3D reconstructions were obtained by using OSIRIX (18) and AMIRA (TGS, San Diego).

The mice (n = 10) were anesthetized with isoflurane gas inhalation during the whole procedure and fixed with tape onto the bedding to reduce possible motion artifacts. Great care was taken to position the mice in the same position as for FMT imaging.

3D volume renderings of the bulk tumor mass were prepared with AMIRA to compare with the 3D renderings of the FMT.

Histology and Immunohistochemistry (IHC). Lungs from tumor-bearing and control animals were inflated with 10% formalin in PBS. After overnight fixation, the lungs were embedded in paraffin, and 4-μm sections were cut and stained with hematoxylin/eosin. IHC was performed on unstained sections with anti-cathepsin H (AF1013), B (AF965), or L (AF952) antibodies (R & D Systems) at 1:100 dilution with the Cadenza buffer system (Shandon, Pittsburgh). Biotinylated secondary antibodies were diluted 1:200 and were detected with horseradish peroxidase by using the VECTASTAIN ABC Kit PK4005 (Vector Laboratories). Slides were counterstained with eosin. Control

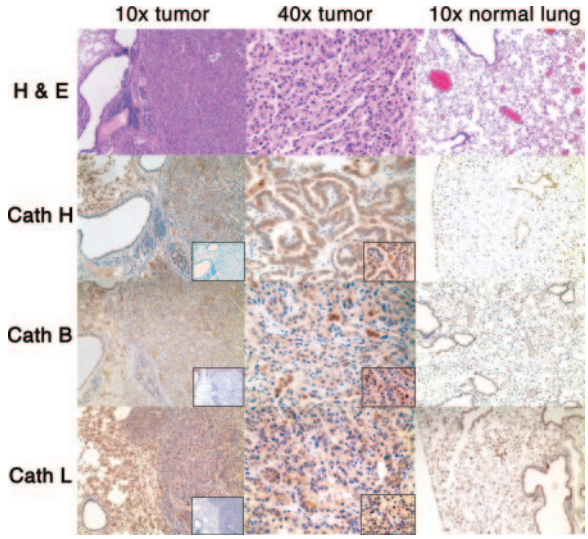

Fig. 1. IHC of lungs from tumor-bearing and control mice show overexpression of cathepsins H, B, and L in tumors. *Insets* in the ×10 IHCs show adjacent slices processed without primary antibody. *Insets* in the ×40 IHCs show ×100 magnification.

sections were processed identically, with the exception of omitting the incubation with the primary antibody.

Western Blot. For immunoblotting, tumors were excised, homogenized in lysis buffer, and subjected to electrophoresis on 12.5 SDS/PAGE followed by transfer to Hybond membrane (Amersham Pharmacia Biosciences) according to the manufacturer's instructions. Concentrations for blotting anti-cathepsin H, B, and L as well as secondary antibodies varied according to the manufacturer's recommendations (R & D Systems and Jackson ImmunoResearch). The blots were developed with the enhanced chemiluminescence system (Amersham Pharmacia Biosciences). Immunoblotting of vinculin was used as a loading control (Sigma).

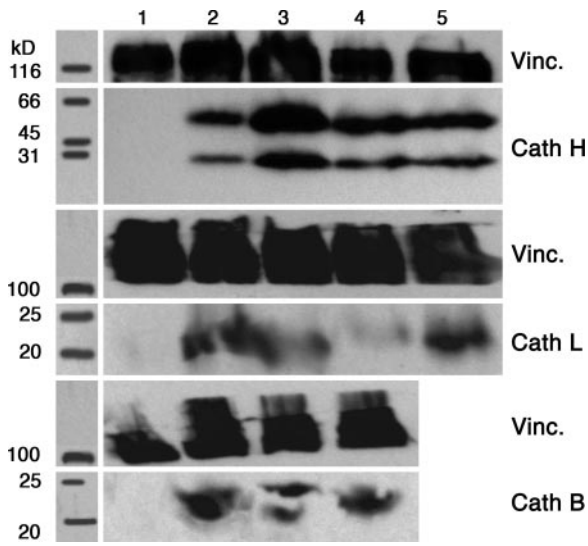

Fig. 2. Immunoblots of lysates of normal lung and from isolated tumors show overexpression of cathepsin H, B, and L protein in tumors. Vinculin immunoblotting was performed as a loading control. Lane 1, lysate from normal lung; lanes 2–5, lysates from different individual tumors. The double signal for cathepsins H and B is due to different glycosylation states of the cathepsin protein.

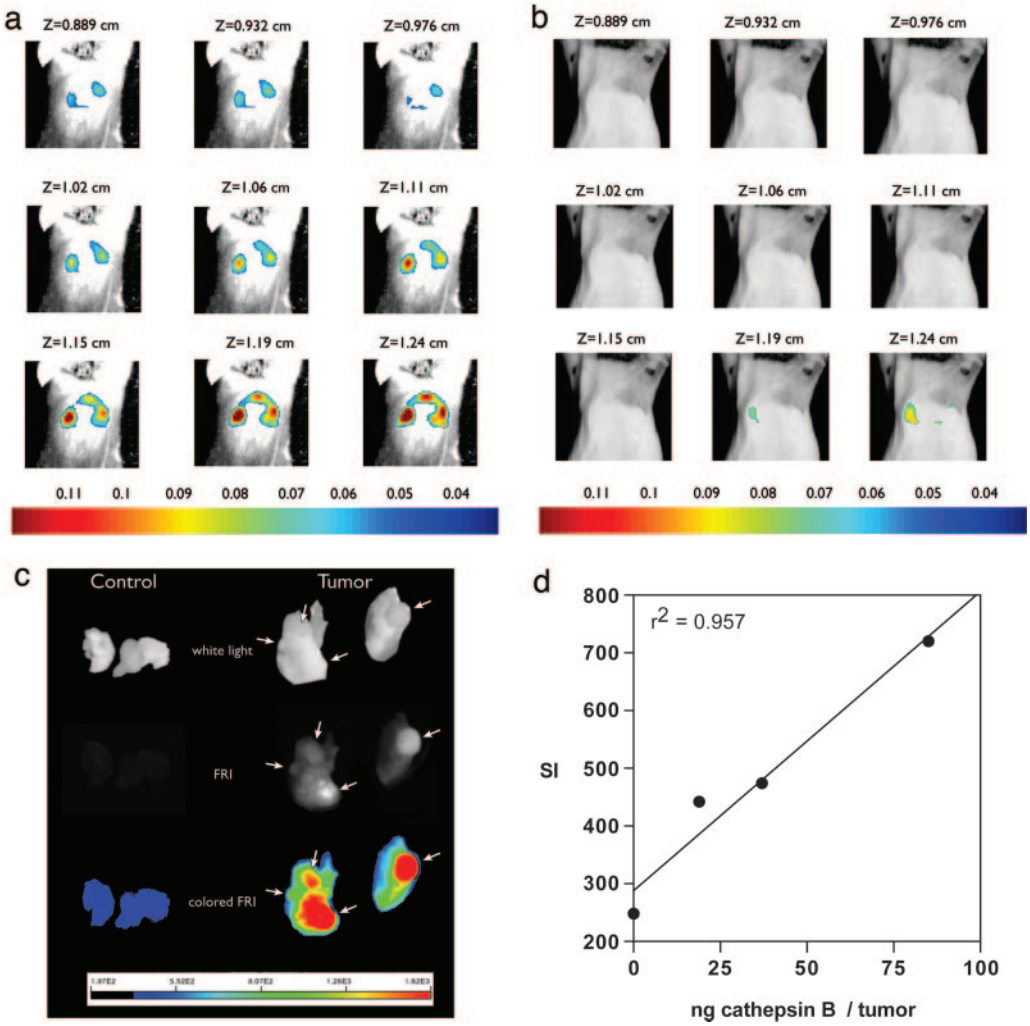

Fig. 3. *In vivo* and *ex vivo* fluorescence imaging of lung tumors. (*a*) FMT identifies lung tumors in mice. The 3D FMT image is displayed at different depths of the coronal plane (*z* axis). The fluorescence signals that are superimposed over the white light image reveal tumors. (*b*) FMT of control mouse shows little fluorescence signal. (*c*) Lung from a mouse with tumor or without tumor (control) was removed 24 h after i.v. injection of probe and imaged with fluorescence reflectance imaging. The fluorescence signal from the control lung is close to the background. In contrast, a clear signal is detectable in tumor-bearing lungs, with the highest signals coming from the areas of macroscopically identifiable tumors indicated (arrows). FRI, fluorescence reflectance image; SI, signal intensity. (*d*) Correlation between the amount of cathepsin B in individually isolated tumors and the corresponding signal intensity by fluorescence reflectance imaging.

Results

We have recently reported that murine lung adenocarcinomas initiated by expressing physiological levels of oncogenic K-rasG12D have a gene expression profile similar to human lung adenocarcinomas (8). Several of the genes overexpressed were cathepsin cysteine proteases, including cathepsins H and B (Table 1). To confirm that these cathepsins were overexpressed in the lung tumors, IHC was performed on sections of paraffin-embedded lungs taken from mice 6 months after Adeno-Cre infection. In lungs from control mice, expression of cathepsins H and B was present in epithelium of bronchi and bronchioles in a lysosomal distribution as previously reported (19) (Fig. 1). In addition, cathepsin H was localized to type II pneumocytes (19). The lung tumors showed increased expression of cathepsins H and B (Fig. 1). Interestingly, normal-appearing lung parenchyma surrounding the tumors also showed increased expression of these proteases compared with lungs obtained from control mice without tumors (Fig. 1). Additional confirmation of increased expression of cathepsins H and B in tumors was obtained by Western blotting. Cathepsin protein levels in normal lungs were below the level of detection in this assay, whereas cathepsin H and B were easily detected in lung tumor lysates (Fig. 2).

The increased expression of cathepsins B and H in lung tumors suggested that the tumors could be imaged by an optical probe activated by these cathepsin proteases. We demonstrated that an optical sensor probe that is known to be activated by cathepsin cysteine proteases was also activatable by cathepsin H (data not shown). We also identified that cathepsin L was overexpressed at the protein level in the lung tumors by IHC and Western blotting (Figs. 1 and 2). Mice that had been infected with Adeno-Cre 6 months before were injected i.v. with the optical probe. Twenty-four hours after injection, cathepsin protease activity was imaged with FMT, allowing fluorescence signals to be resolved in three dimensions. A significantly higher fluorescence signal was obtained from mice with lung tumors (Fig. 3*a*) than from control mice (Fig. 3*b*). Remarkably, the fluorescence signal was found to originate from areas deep within the lung parenchyma. To verify that the cathepsin signal originated from lung tumors, the lungs were excised and imaged again with reflectance imaging (Fig. 3*c*). Unlike FMT, which resolves fluorescence signal in three dimensions, reflectance imaging is

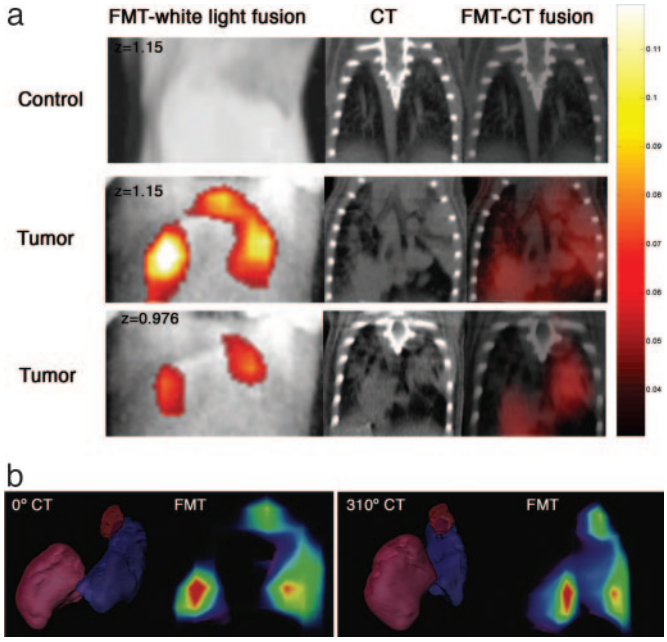

Fig. 4. Comparison of FMT and CT images of lung tumors. (*a*) FMT-white light fusion, CT, and FMT-CT fusion images of a tumor-bearing mouse (two slices at different depths) and of a control mouse (one position). (*b*) 3D reconstructions of the bulk tumor mass in CT (*Left*) and of the FMT signal (*Right*) show a good correlation.

surface-weighted, so that fluorescence signal is most easily detected on the surface. Whereas control lungs had signal intensities near background, the reflectance imaging of lungs from tumor-bearing mice showed a significant increase of signal intensities ($P = 0.018$), most pronounced over visible tumors (arrows in Fig. 3*c*). The fluorescence signal intensity in individually excised tumors correlated well with the amount of cathepsin B within each tumor as determined by Western blot ($r^2 = 0.957$; Fig. 3*d*).

To evaluate whether the location of the cathepsin activity by optical imaging correlated with the anatomical location of lung tumors, mice with lung tumors were imaged by CT before optical imaging. CT is a standard method for imaging lung cancer in patients. We used a micro-CT with a voxel resolution of 72 microns, which can therefore detect lung tumors with submillimeter resolution (Fig. 6, which is published as supporting information on the PNAS web site). After manually coregistering the coronal images from CT with those from FMT, the fluorescence signal colocalized with the anatomical location of the tumor masses by micro-CT (Fig. 4; see also Movies 1 and 2, which are published as supporting information on the PNAS web site). Therefore, by using an optical probe that is activated by proteases overexpressed in lung cancers, optical imaging successfully detects these primary lung cancers in mice.

To establish the limits of detection of tumors with FMT, we imaged mice 11 weeks after infection with Adeno-Cre (Fig. 5*a*). At this time point, we found that the fluorescence signal identified some, but not all, areas with tumor. In the coronal image displayed in Fig. 5*a*, fluorescence activity detected the right-sided tumors (white arrows), which ranged in maximal axial diameter from 0.93 to 1.3 mm. However, the left-sided tumor (red arrow), with an axial diameter of 0.7 mm, could not be detected with this scanner and our current reconstruction algorithm.

We next determined whether FMT could be used to measure tumor progression. Lung tumors in the LSL-KrasG12D model

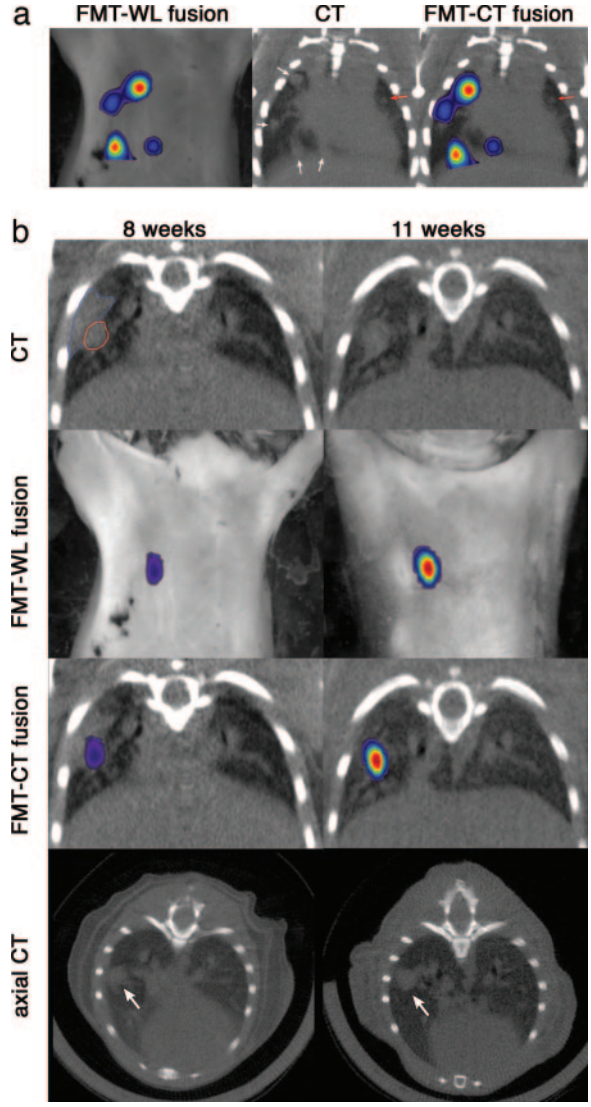

Fig. 5. FMT of mice demonstrating the limits of tumor detection and serial imaging of tumor progression. (*a*) Limits of tumor detection: FMT-white light (WL) fusion, CT, and FMT-CT fusion images 11 weeks after infection with Adeno-Cre show that some tumors (white arrows) can be detected by FMT but that a smaller individual tumor (red arrow) cannot be detected. (*b*) Tumor progression: Coronal CT, FMT-WL fusion, CT-FMT fusion, and axial CT images through the tumor (arrow) of the same LSL-KrasG12D mouse 8 and 11 weeks after Adeno-Cre infection. Serial imaging of the same mouse with FMT over time detects tumor progression. The structure outlined in blue in the coronal CT image at 8 weeks is a pleural effusion that has resolved by 11 weeks; the tumor is outlined in red.

have previously been shown to progress from adenomas to adenocarcinomas over a time course of 6–16 weeks after Adeno-Cre infection (2). Therefore, we serially imaged LSL-KrasG12D mice with CT and FMT. At 8 weeks after Adeno-Cre infection, lung tumors could be detected with CT and FMT (Fig. 5*b*). By 11 weeks, not only had the tumors increased in size as measured by CT (from 1.7 to 2.4 mm), but the fluorescence signal had increased with tumor progression as well (Fig. 5*b*).

The increased fluorescence signal during tumor progression correlated with an increased tumor size on CT. However, the increased fluorescence signal may also reflect higher levels of cathepsin protease activity within the tumor if the level of fluorescence is proportional to cathepsin protease activity. Indeed, the fluorescence signal intensity in individually excised

tumors shown in Fig. 3*c* correlated well with the amount of cathepsin B within each tumor as determined by Western blot ($r^2 = 0.957$; Fig. 3*d*).

Discussion

Using gene expression profiling of lung tumors expressing physiological levels of oncogenic K-rasG12D, we have identified overexpression of cathepsin cysteine proteases H and B. We have confirmed overexpression of these proteases at the protein level by IHC and Western blot of the lung tumors.

Although cathepsin L was not overexpressed at the mRNA level by gene expression analysis, IHC and Western blot of the lung tumors did show overexpression of cathepsin L at the protein level. We found that an optical probe whose fluorescence is known to be dequenched after cleavage by cathepsin proteases B, L, and S was also activatable by cathepsin H *in vitro*. Using this information, we selected this optical probe to image primary lung tumors in living mice.

We found that FMT could be used to detect tumors deep within the lung parenchyma. The location of the fluorescence signals in the optical image of the lung tumor mass corresponded with their anatomical location on CT, demonstrating the potential value of molecular imaging as a potential diagnostic tool for lung cancer.

We also imaged mice at an early stage of tumor development, when some tumors were below the resolution of this system. For example, tumors ranging in maximal diameter from 0.93 to 1.3 mm could be detected. However, individual tumors with a maximal diameter of 0.7 mm or less could not be detected in the same animal, which likely represents a threshold of tumor detection with this system. When multiple tumors of this size are in close proximity to each other, however, it is possible to detect the bulk tumor mass as a fluorescent signal. Future developments in technology, reconstruction algorithms, and imaging probes promise to increase the resolution of FMT with the next generation of optical tomographic scanners even further.

In addition, we have shown that it is feasible to serially image the same mouse over time with FMT, which allowed us to use optical imaging to detect tumor progression.

Interestingly, we also observed up-regulation of cathepsins B, H, and L in the normal-appearing lung parenchyma in mice with lung tumors. Similar results have been reported in patients with lung adenocarcinoma. For example, cathepsin H is overexpressed at the RNA and protein levels in normal-appearing lung adjacent to lung adenocarcinomas (15). Because cathepsin protease activity appears increased in the tumor as well as the adjacent normal-appearing lung, this finding raises a potential paradox of why the signal is higher in areas with tumors. This paradox can likely be explained by the relative difference in air space in tumor-bearing versus normal lung. Therefore, in normal-appearing lung, there is increased cathepsin protease expression at the single-cell level, but for a given volume of lung that is largely made up of air, there is relatively little protease activity compared with the same volume filled with densely packed tumor cells overexpressing cathepsin proteases.

Overexpression of cathepsin proteases in lung adenocarcinomas has previously been observed in patients. Remarkably, cathepsin B has consistently been shown to be an independent prognostic factor of poor outcome in patients with lung adenocarcinoma (20), colorectal cancer (21), pancreatic adenocarcinoma (14, 22), and oral squamous cell carcinoma (23). Recently, cathepsin B was also found to be a predictor of prostate cancer that extends beyond the prostate gland (24). Many human lung adenocarcinomas also have been found to overexpress cathepsin H (15, 25). Cathepsin L has been reported to be an independent prognostic factor for poor outcome in some studies (22) but not in others (20, 23). Interestingly, cathepsin L was recently identified as one of six genes predicting metastasis in patients with breast cancer (26). Cathepsin cysteine proteases have been implicated in tumor invasion and metastasis (14). Taken together, these studies suggest that cathepsin cysteine proteases play an important role in lung cancer prognosis. Therefore, imaging cathepsin protease activity of lung cancers by optical imaging (during bronchoscopy, for example) could potentially provide important diagnostic information.

In summary, by using gene expression profiling, we found that cathepsin cysteine proteases are overexpressed in murine lung adenocarcinomas. After confirming overexpression at the protein level, we selected an optical probe to image these tumors. The lung tumors were successfully visualized by using 3D optical imaging; the anatomical location of the signal correlated with tumor location by micro-CT. By imaging mice with tumors at an early stage of development, we established the limits of detection with this optical imaging system. Furthermore, serial imaging demonstrated that FMT can monitor tumor progression in the same mouse. Finally, this study demonstrates how gene expression profiling of tumors can be used to select molecular imaging techniques in mice that may be applicable for the detection of cancer.

We thank Peter Waterman and Gregory Wojtkiewicz for technical support and Alejandro Sweet-Cordero for helpful discussions. This work was supported in part by National Cancer Institute Grants P50 CA86355, P01 CA69246, R2492782, and R33 CA91807 (to R.W.); an American Society of Clinical Oncology Young Investigator Award (to D.G.K.); and a Radiological Society of North America Holman Pathway Seed Grant (to D.G.K.). T.J. is a Howard Hughes Medical Institute Investigator.

1. Branda, C. S. & Dymecki, S. M. (2004) *Dev. Cell* **6,** 7–28.
2. Jackson, E. L., Willis, N., Mercer, K., Bronson, R. T., Crowley, D., Montoya, R., Jacks, T. & Tuveson, D. A. (2001) *Genes Dev.* **15,** 3243–3248.
3. Pelosi, G., Scarpa, A., Manzotti, M., Veronesi, G., Spaggiari, L., Fraggetta, F., Nappi, O., Benini, E., Pasini, F., Antonello, D., *et al.* (2004) *Mod. Pathol.* **17,** 538–546.
4. Okudela, K., Hayashi, H., Ito, T., Yazawa, T., Suzuki, T., Nakane, Y., Sato, H., Ishi, H., KeQin, X., Masuda, A., *et al.* (2004) *Am. J. Pathol.* **164,** 91–100.
5. Kim, D. H., Kim, J. S., Park, J. H., Lee, S. K., Ji, Y. I., Kwon, Y. M., Shim, Y. M., Han, J. & Park, J. (2003) *Cancer Res.* **63,** 6206–6211.
6. Tuveson, D. A., Shaw, A. T., Willis, N. A., Silver, D. P., Jackson, E. L., Chang, S., Mercer, K. L., Grochow, R., Hock, H., Crowley, D., *et al.* (2004) *Cancer Cell* **5,** 375–387.
7. Johnson, L., Mercer, K., Greenbaum, D., Bronson, R. T., Crowley, D., Tuveson, D. A. & Jacks, T. (2001) *Nature* **410,** 1111–1116.
8. Sweet-Cordero, A., Mukherjee, S., Subramanian, A., You, H., Roix, J. J., Ladd-Acosta, C., Mesirov, J., Golub, T. R. & Jacks, T. (2005) *Nat. Genet.* **37,** 48–55.
9. Weissleder, R. (1999) *Radiology* **212,** 609–614.
10. Tung, C. H., Mahmood, U., Bredow, S. & Weissleder, R. (2000) *Cancer Res.* **60,** 4953–4958.
11. Ntziachristos, V., Tung, C. H., Bremer, C. & Weissleder, R. (2002) *Nat. Med.* **8,** 757–760.
12. Ntziachristos, V., Bremer, C., Graves, E. E., Ripoll, J. & Weissleder, R. (2002) *Mol. Imaging* **1,** 82–88.
13. Ntziachristos, V., Ripoll, J., Wang, L. V. & Weissleder, R. (2005) *Nat. Biotechnol.* **23,** 313–320.
14. Joyce, J. A., Baruch, A., Chehade, K., Meyer-Morse, N., Giraudo, E., Tsai, F. Y., Greenbaum, D. C., Hager, J. H., Bogyo, M. & Hanahan, D. (2004) *Cancer Cell* **5,** 443–453.
15. Schweiger, A., Staib, A., Werle, B., Krasovec, M., Lah, T. T., Ebert, W., Turk, V. & Kos, J. (2000) *Br. J. Cancer* **82,** 782–788.
16. Olive, K. P., Tuveson, D. A., Ruhe, Z. C., Yin, B., Willis, N. A., Bronson, R. T., Crowley, D. & Jacks, T. (2004) *Cell* **119,** 847–860.
17. Montet, X., Ntziachristos, V., Grimm, J. & Weissleder, R. (2005) *Cancer Res.* **65,** 6330–6336.
18. Rosset, A., Spadola, L. & Ratib, O. (2004) *J. Digit. Imaging* **17,** 205–216.

19. Ishii, Y., Hashizume, Y., Watanabe, T., Waguri, S., Sato, N., Yamamoto, M., Hasegawa, S., Kominami, E. & Uchiyama, Y. (1991) *J. Histochem. Cytochem.* **39,** 461–468.
20. Kayser, K., Richter, N., Hufnagl, P., Kayser, G., Kos, J. & Werle, B. (2003) *Anticancer Res.* **23,** 2767–2772.
21. Guzinska-Ustymowicz, K., Zalewski, B., Kasacka, I., Piotrowski, Z. & Skrzydlewska, E. (2004) *Anticancer Res.* **24,** 2847–2851.
22. Niedergethmann, M., Wostbrock, B., Sturm, J. W., Willeke, F., Post, S. & Hildenbrand, R. (2004) *Pancreas* **29,** 204–211.
23. Kawasaki, G., Kato, Y. & Mizuno, A. (2002) *Oral Surg. Oral Med. Oral Pathol. Oral Radiol. Endod.* **93,** 446–454.
24. Miyake, H., Hara, I. & Eto, H. (2004) *Anticancer Res.* **24,** 2573–2577.
25. Bhattacharjee, A., Richards, W. G., Staunton, J., Li, C., Monti, S., Vasa, P., Ladd, C., Beheshti, J., Bueno, R., Gillette, M., *et al.* (2001) *Proc. Natl. Acad. Sci. USA* **98,** 13790–13795.
26. Paik, S., Shak, S., Tang, G., Kim, C., Baker, J., Cronin, M., Baehner, F. L., Walker, M. G., Watson, D., Park, T., *et al.* (2004) *N. Engl. J. Med.* **351,** 2817–2826.